IEEE Access
Multidisciplinary | Rapid Review | Open Access Journal

Received February 8, 2019, accepted February 26, 2019, date of publication March 4, 2019, date of current version March 29, 2019.

Digital Object Identifier 10.1109/ACCESS.2019.2902576

Quantitative Detection of Living Yeast Fraction From Mixed Living and Dead Cell Solution by Micro Electrical Impedance Spectroscopy

XIAYI LIU[1], YAHUI CUI[1], TONG ZHAO[1], DAISUKE KAWASHIMA[2], HIROMICHI OBARA[3], AND MASAHIRO TAKEI[2], (Member, IEEE)

[1]Faculty of Mechanical and Precision Instrument Engineering, Xi'an University of Technology, Xi'an 710048, China
[2]Department of Mechanical Engineering, Chiba University, Chiba 263-0022, Japan
[3]Department of Mechanical Engineering, Tokyo Metropolitan University, Tokyo 192-0397, Japan

Corresponding author: Tong Zhao (tongzhao@xaut.edu.cn)

This work was supported in part by the National Natural Science Foundation of China under Grant 51506175, in part by the Bio Assembler, Grant-in-Aid for Scientific Research on Innovative Areas of Japan, under Grant 26106708, and in part by the Innovative Talents Promotion Project of Shaanxi Province, China, under Grant 2018KJXX-067.

ABSTRACT An empirical model is proposed to detect the living cell fraction Φ in a multi-mixed cell solution by micro electrical impedance spectroscopy (EIS) as $\Phi = -1.46/\psi_0 + 1.97$. The living cell indicator ψ_0 is defined by a quotient of the extrema in the impedance imaginary parts of the detected cell solution's medium, Z_{extmed}, and referenced $Z_{extmedref}$. The theoretical effectiveness of the model is examined by an electrochemical simulation. In addition, the sensor size versatility is discussed by a comparison experiment that reveals that the sensor size has little effect on the detection result. To support real-time detection, Z_{extmed} and $Z_{extmedref}$ are replaced by the impedance of the cell solution, Z_{extm}, and $Z_{extmref}$. The versatility of real-time detection is discussed by a medium similarity coefficient $\eta(f)$ that is defined to explain the effect of replacement. The results reveal the feasibility of the replacement as $\eta > 95\%$ in the injected current frequency range of ψ_0 by micro EIS.

INDEX TERMS Micro electrical impedance spectroscopy, yeast cell solution, quantitative detection of living cell fraction.

I. INTRODUCTION

Quantitative detection of one kind of cell fraction in a multi-mixed cell solution is an innovative future technology for cell engineering when assembling cells for organ reconstruction and diagnosing cell-related diseases [1]. Despite the technology, the qualitative distinction of one kind of cell in a multi-mixed cell solution remains a problem wherein it is not easy to quantitatively detect one kind of cell fraction. The qualitative distinction method of cancerous cells from normal cells in nutrient solutions is typically studied by ideas such as CT and other invasive chemical label method [2], [3]. MTT assay and flow cytometry are mature methods to quantitative detect normal cells fraction in a mixed cell solution [4], [5]. However, these methods labeled cell by staining and affect the cells functions.

The associate editor coordinating the review of this manuscript and approving it for publication was Lei Wang.

Meanwhile, an electrical detection method such as electrical impedance spectroscopy (EIS) is a featured idea to investigate cells' electrical behavior and to distinguish the abnormal cells [6], [7]. The complex electrical impedance which is estimated by EIS provides the compositional and structural properties as well as the electrical properties of the materials [8], [9]. EIS is an effective diagnostic tool as it is fast, sensitive, safe, nonintrusive, label-free, and does not modify the cells [10].

Recently, the application of EIS in micro sensors, which is called micro EIS, has a high advantage in distinguishing qualitatively abnormal and normal cells in a small amount of cell solution or tissues. For instance, Kang *et al.* [6] (2012) distinguished cancer cells in breast, prostate, and bladder tissues by micro EIS. Han *et al.* [11] (2006) designed a special micro sensor to analyze the breast cancer cells in static blood by micro EIS. Yun *et al.* [12] (2016) integrated micro finger electrodes on a needle (μEoN) to qualitatively distinguish

cancer cells from human renal tissues by micro EIS. The authors of this paper already proposed a visualization method for cell distribution in a micro sensor by micro EIS and micro electrical impedance tomography (EIT) to discuss a downsizing effect [13].

However, these micro EIS research studies focused on the qualitative distinction of abnormal single cells or tissues. Few researchers have studied the quantitative detection of one kind of cell fraction in a multi-mixed cell solution by micro EIS. The quantitative detection is effective in qualifying the properties of the cell solution as to whether the cells are acceptable in recycling and cultures [14], [15].

In this study, an approach to the quantitative detection of cells fraction in multi-mixed cell solution is based on the impedance of the medium of the multi-mixed cell solution. The ion release rate of abnormal cells such as dead cells is different from the ion release rate of normal cells [16]–[18]. The relation between the ion concentration and conductivity is expressed as the molar conductivity in current studies [19]. The theory of molar conductivity is created based on the condition of the electrolyte. However, the suitability of the detection method on the cell solution in micro detection is not clear. It is necessary to investigate the relation between the ion concentration and solution conductivity of a multi-mixed cell solution. In addition, it is required that the effect of the sensor size on this relation is investigated to extend the versatility of the detection method. Meanwhile, the medium is not easy to extract during real-time detection. To support real-time detection, the medium is replaced by a cell solution. The effect of the replacement is important because it reveals the accessibility and practicability of the detection.

This paper proposes a novel quantitative detection of living yeast cells fraction in a multi-mixed living and dead cell solution by micro EIS. Firstly, an indicator of the living cell fraction is defined as a main concept of the proposed method. The principle of the fitting empirical equation is explained. Secondly, experiments by micro EIS are conducted on the multi-mixed cell solution to prove the proposed method. Thirdly, the relation between the ion concentration and conductivity of the solution is numerically simulated to prove theoretically the effectiveness of the proposed method. In addition, the detection versatility is discussed from two perspectives: the sensor size versatility is discussed by a comparison experiment with a macro sensor, and the versatility of real-time detection is investigated by the effect of replacing the medium with a cell solution.

II. PRINCIPLE OF DETECTING LIVING CELLS FRACTION

The living cell indicator ψ_0 is newly defined as a quotient of two extrema from the impedance imaginary part against the injected current frequency f in the cell solution's medium, as shown in **FIGURE 1. (a)**. This indicator is expressed as follows:

$$\psi_0 = \frac{Z''_{extmed}}{Z''_{extmedref}} \tag{1}$$

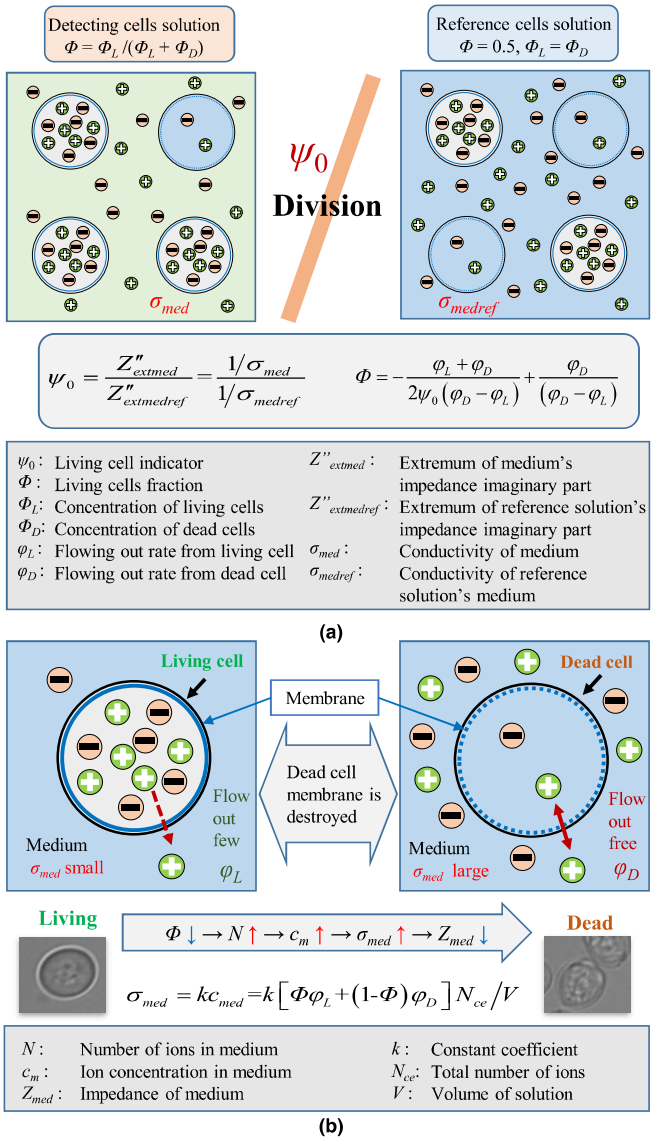

FIGURE 1. **Methods of principle: (a) Method of relation between Φ and ψ_0. (b) Models of living and dead cells and relation between σ_m and c_m.**

where Z''_{extmed} [Ω] is the extremum of the impedance imaginary part from the detected cell solution's medium. The medium of the cell solution is supernatant and is extracted after centrifuging the cell solution. $Z''_{extmedref}$ [Ω] is the extremum of the impedance imaginary part from the referenced cell solution's medium. The referenced cell solution is mixed with the same concentration of living and dead cells.

In **FIGURE 1. (a)**, the cell living indicator ψ_0 [−] has a relation to the living cell fraction Φ [−] in the multi-mixed living and dead cell solution. The referenced solution is adopted as a standard to eliminate the unknown coefficients to simplify the detection. It is expressed as follows:

$$\Phi = -\frac{\varphi_L + \varphi_D}{2\psi_0(\varphi_D - \varphi_L)} + \frac{\varphi_D}{(\varphi_D - \varphi_L)} = a/\psi_0 + b \tag{2}$$

where φ_L is the ion release rate from the living cells, and φ_D is the ion release rate from the dead cells. $\varphi_D > \varphi_L$ because

ions in the dead cell have no limit on release, and most of the ions in the living cells are limited on release by the membrane. a and b are constant coefficients that are calculated by fitting the experimental data because the values of φ_D and φ_L are not easy to detect. Φ is defined as follows:

$$\Phi \equiv \Phi_L / (\Phi_L + \Phi_D) \tag{3}$$

where Φ_L [vol%] is the volume concentration of living cells in the multi-mixed cell solution, and Φ_D [vol%] is the concentration of dead cells in the multi-mixed cell solution. $\Phi_{total} = \Phi_L + \Phi_D$, and Φ_{total} [vol%] is the concentration of total living and dead cells in the multi-mixed cell solution. The range of Φ is $0 < \Phi < 1$. In this study, the reference solution is defined as $\Phi_L = \Phi_D$.

Z''_{extmed} and $Z''_{extmedref}$ are calculated as follows:

$$Z''_{extmed} = \frac{d}{2A\sigma_{med}}$$
$$Z''_{extmedref} = \frac{d}{2A\sigma_{medref}} \tag{4}$$

where σ_{med} [S/m] is the conductivity of the detected cell solution's medium, and σ_{medref} [S/m] is the conductivity of the referenced cell solution's medium. d [m] is the distance between two electrodes, and A [m^2] is the surface area of the electrodes.

Simplified models of the living and dead cells are shown in **FIGURE 1. (b)**. The living cell has a membrane that protects the cell cytoplasm and limits most of the ions from releasing from the cell. This reveals that φ_L is small (living cells release few ions when metabolizing). In the case of the dead cells, the ions in the dead cells release freely ($\varphi_D > \varphi_L$) because the membrane is destroyed. As a result, in the mixed living and dead cell solution, while Φ decreases, more ions are released into the medium, N (the number of ions in the medium) is increased, c_m [mol/L] (the ion concentration in the medium)is increased, σ_{med} (the conductivity of the medium) is increased, and Z_{med} [Ω] (the impedance of the medium) is decreased [20].

When c_m is small (the ions have no limit of dilution), the relation of c_m and σ_{med} is treated as linear (details are provided in the Discussion section) [21]. The relation between σ_{med} and Φ is expressed as follows:

$$\sigma_{med} = kc_m = k[\Phi\varphi_L + (1-\Phi)\varphi_D]N_{ce}/V \tag{5}$$
$$\sigma_{medref} = kc_{mref} = k[\varphi_L + \varphi_D]N_{ce}/2V \tag{6}$$

where k is a constant coefficient, and N_{ce} is the total number of ions in the cells and cell solution. V [m^3] is the volume of the cell solution. Eq. (2) is expressed as the quotient of Eq. (5) and Eq. (6).

III. EXPERIMENTS

A. EXPERIMENTAL SETUPS

FIGURE 2. shows the experimental setups for micro EIS. The setups consist of a multilayered microchannel, syringe pump (Muromachi KDS-100), Faraday cage, impedance analyzer (HIOKI IM3570) that supports a scanning frequency range from 4 Hz to 5 MHz, and a PC (Mouse computer W950JU). The structure of a microchannel is shown under the setups, and the average distance between two electrodes is $d_s = 350\ \mu$m. In this section, the thickness of the electrode is $k_t = 10\ \mu$m, and its width is $w_t = 200\ \mu$m. The photographs are of a microchannel and micro computed tomography (CT) image of one cross section in the microchannel (obtained by X-ray CT scanner model TDM1300-IS, Yamato Scientific, Japan) [22]–[24].

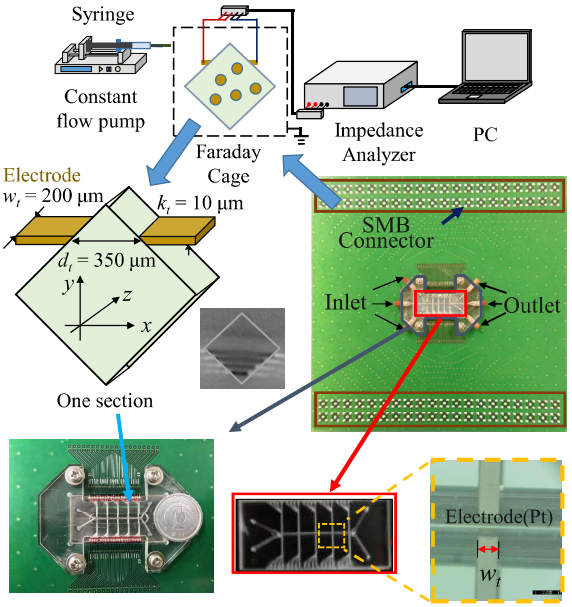

FIGURE 2. Experimental setups.

B. EXPERIMENTAL METHODS

Mediums of the solution are achieved as a sample by extracting the supernatant from the centrifuged cell solution. It is useless and unsupported for real-time detection. In order to support the real time detection, the process of extracting the medium from the cell solution is canceled. Approximately, the impedances of cell medium Z_{extmed} and $Z_{extmedref}$ are replaced by the impedance of cell solution Z_{extm} [Ω] and $Z_{extmref}$ [Ω]. The conductivities of the medium (σ_{med} and σ_{medref}) are replaced by the conductivities of the cell solution (σ_m and σ_{mref}). This is expressed as follows:

$$\psi_0 = \frac{Z''_{extmed}}{Z''_{extmedref}} = \frac{Z''_{extm}}{Z''_{extmref}} \tag{7}$$

From Eqs. (1) and (7), the empirical equation of $\Phi(\psi_0)$ is fitted by the experiment results. ψ_0 is achieved by calculation: divide each Z''_{extm} by the referenced $Z''_{extmref}$ (in the case of $\Phi = 0.5$). The empirical equation is fitted by the least square method, and R^2 is employed to evaluate the accuracy of the equation.

C. EXPERIMENTAL CONDITIONS

The measurement objects of the experiments were mixed in different concentrations of living and dead yeast cell solution. The yeast cell solution was cultured by yeast and pure water for $t = 30$ min at a constant temperature $T_1 = 298$ K,

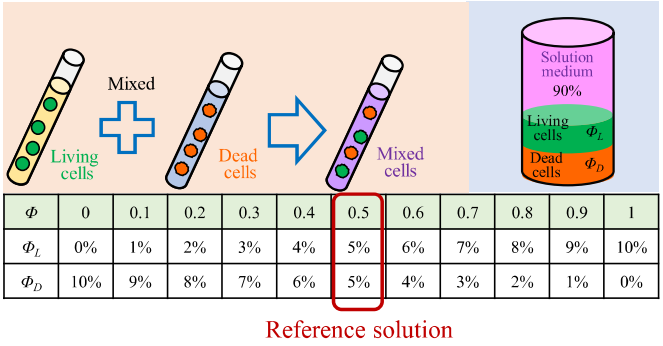

Φ	0	0.1	0.2	0.3	0.4	0.5	0.6	0.7	0.8	0.9	1
Φ_L	0%	1%	2%	3%	4%	5%	6%	7%	8%	9%	10%
Φ_D	10%	9%	8%	7%	6%	5%	4%	3%	2%	1%	0%

Reference solution

FIGURE 3. Conditions of mixed cell solution in experiment.

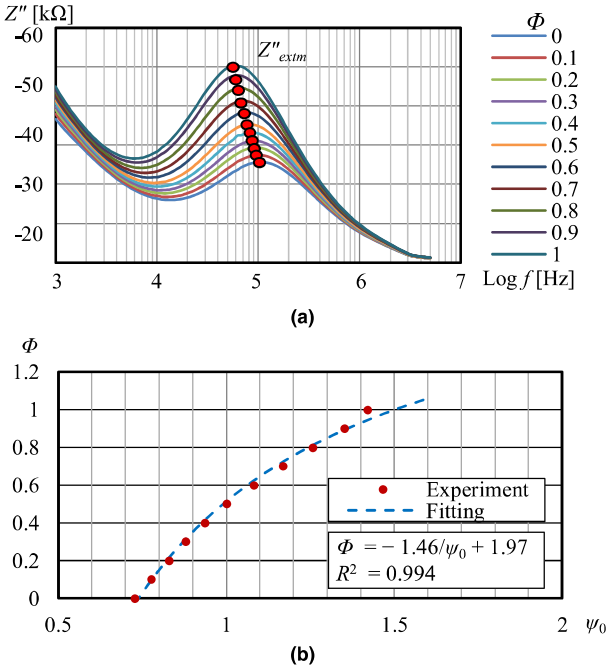

FIGURE 4. Experiment results. (a) Z'' by f in micro EIS. (b) $\psi_0 - \Phi$ and fitting equation.

and the dead cells were processed by putting living cells into hot water ($T_2 = 363$ K) for 5 min. The different concentrations of cell solution are shown in **FIGURE 3.** The volume concentration of the multi-mixed cell solution was $\Phi_{total} = \Phi_L + \Phi_D = 10$ vol%. The concentrations of living cells were $\Phi = 0$, 0.1, 0.2, 0.3, 0.4, 0.5, 0.6, 0.7, 0.8, 0.9 and 1. The reference solution is $\Phi = 0.5$. The applied alternate current was $i_C = 0.1$ mA. The injected current frequency range was from 1 kHz to 5 MHz.

D. EXPERIMENT RESULTS

FIGURE 4. (a) shows the results measured by micro EIS. The horizontal axis is the logarithm expression of the injected current frequency f, and the vertical axis is the imaginary part of the impedance. The red points are extrema in each Φ. In the injected current frequency range between $f = 1$ kHz to $f = 10$ kHz, Z'' is large and decreases as f increases. This phenomenon is caused by the contact impedance. In the range of f between $f = 20$ kHz to $f = 5$ MHz, Z'' is increased to an extremum (red point in each Φ) and then decreased in each Φ. The extrema is increased as Φ is increased, which reveals that the conductivity of the cell solution is decreased.

FIGURE 4. (b) shows a chart of $\psi_0 - \Phi$ by micro EIS. The horizontal axis is ψ_0, and vertical axis is Φ. The red points are the calculated ψ_0 in each Φ by the result of micro EIS. The blue dotted line indicates the fitted experiment equation by the least square method from the five red points of ψ_0 in **FIGURE 4. (a)**. From the chart, as ψ_0 is increased, Φ is increased.

The empirical equation of the relation between ψ_0 and Φ is fitted by least squares as follows:

$$\Phi = a/\psi_0 + b = -1.46/\psi_0 + 1.97 \tag{8}$$

where the coefficients $a = -1.46$, $b = 1.97$, and $R^2 = 0.994$.

IV. DISCUSSIONS

A. SIMULATION OF RELATIONSHIP BETWEEN LIVING CELL INDICATOR AND LIVING CELL FRACTION

An empirical equation develops an effective method for the detection of the living cell fraction in a mixed living and dead cell solution. However, as addressed in Eq. (5) and Eq. (6), the relation between the ion concentration and conductivity of the medium is treated as linear, which is the theoretical effectiveness of the proposed method. A numerical simulation is employed to discuss its rationality.

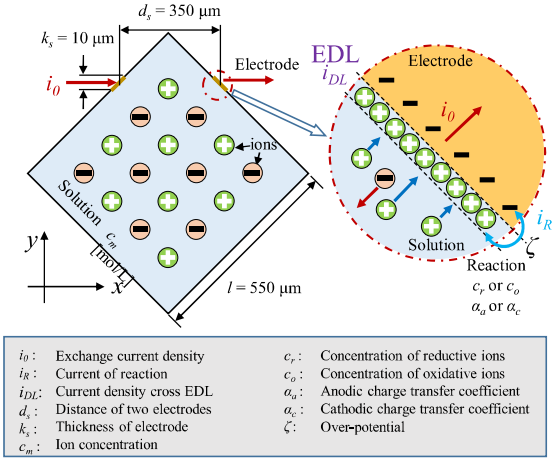

FIGURE 5. Simulation model.

FIGURE 5. shows a simulation model that has the same size as the microchannel in the experiment. The length of the two electrodes is $k_s = 10$ μm. The average distance between the two electrodes is $d_s = 350$ μm. Ions are distributed evenly in the simulation domain.

The relation between the conductivity of ion solution σ_m and ion concentration c_m is expressed as follows [25]:

$$\sigma_m = \frac{j\omega\zeta C_{DL} + i_0\left[c_r \exp\left(\frac{\alpha_a F\zeta}{RT}\right) - c_o \exp\left(\frac{\alpha_c F\zeta}{RT}\right)\right]}{-\nabla\zeta} \tag{9}$$

where ω is defined as $\omega = 2\pi f$, f is the injected current frequency, ζ [V] is the overpotential (the difference between the applied potential and equilibrium potential of the redox couple of species), C_{DL} is the capacitance density of the electrical

TABLE 1. Parameters of simulation.

Symbol	Quantity	Unit	Value
c_m	Ion concentration	mol/L	0.1 to 0.2
f	Injected current frequency	Hz	1 k to 10 M
ζ	Overpotential	V	5
i_0	Exchange current density	A/m^2	100
C_{DL}	Capacitance of EDL	μF/cm^2	20
c_r	Concentration of reductive	mol/L	0.5c
c_o	Concentration of oxidative	mol/L	0.5c
α_a	Anodic charge transfer	-	0.5
α_c	Cathodic charge transfer	-	0.5
R	Gas constant	J/(Kmol)	8.314
T	Absolute temperature	K	293.15

double layer (EDL), i_0 is the exchange current density, and c_r [mol/L] and c_o [mol/L] are the concentration of reductive and oxidative ions ($c_m = c_r + c_o$), respectively. α_a and α_c are anodic and cathodic charge transfer coefficients, F [C/mol] is the Faraday constant, T [K] is the absolute temperature, and R [J/(mol·K)] is the gas constant.

Based on Ohm's law, the total current density i_{to} [A/m^2] through the electrode is expressed as follows:

$$i_{to} = -\sigma_m \nabla\zeta \tag{10}$$

In the present simulation, i_{to} is defined as the summation of the current density through the EDL i_{DL} [A/m^2] and that of the electrode reaction i_R [A/m^2]. This is expressed as follows:

$$i_{to} = i_{DL} + i_R \tag{11}$$

i_{DL} and i_R are expressed as follows:

$$i_{DL} = j\omega\zeta C_{DL} \tag{12}$$

$$i_R = i_0\left[c_r \exp\left(\frac{\alpha_a F\zeta}{RT}\right) - c_o \exp\left(\frac{\alpha_c F\zeta}{RT}\right)\right] \tag{13}$$

In addition, the idea of a living cell indicator ψ_0 is employed to simulate the tendency of the relation between ψ_0 and c_m. The living cell indicator in the simulation is defined as ψ_1, which is expressed as follows:

$$\psi_1 = \frac{Z''_{ext}}{Z''_{extref}} \tag{14}$$

where Z''_{ext} is the extremum of Z'', and Z''_{extref} is the extremum of Z''_{red}, which is defined as the condition of $c_m = 0.15$ mol/L.

The relation between Φ and c_m from Eq. (5) is expressed as follows:

$$c_m = k'\Phi\,(\varphi_L - \varphi_D) + k'\varphi_D \tag{15}$$

where k' is a constant coefficient. The relation between Φ and ψ_1 is expressed as Eq. (2). The conditions of the simulation are defined in TABLE 1 [26]–[28]. $c_r = c_o = 0.5\ c_m$, and the range of c_m is defined as from $c_m = 0.1$ mol/L to $c_m = 0.2$ mol/L at an interval of 0.01 mol/L, for a total of 11 swapped points.

FIGURE 6. (a) shows a Nyquist plot of the solution with different ion concentrations. In **FIGURE 6. (a)**, the straight line at low frequency is caused by the contact impedance, and the semicircle at high frequency is caused by the ions in the solution. It is clear that when c_m increases, the radii of

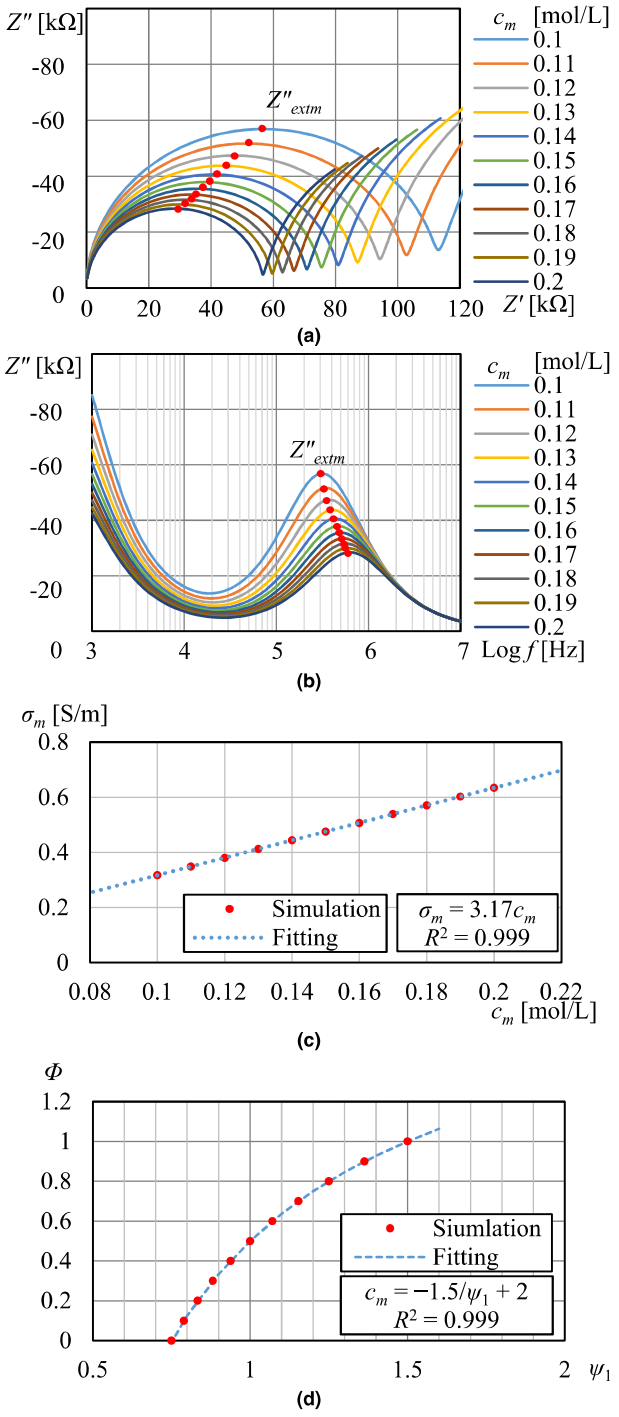

FIGURE 6. Simulation results. (a) Nyquist plot. (b) Bode plot. (c) $c_m - \sigma_m$ and fitting equation. (d) $\psi_1 - \Phi$ and fitting equation.

the semicircles are decreased. **FIGURE 6. (b)** shows a Bode plot that replenishes the change in Z'' by f.

As shown in **FIGURE 6. (b)**, the extremum of Z'' (the red points in each curve) at high frequency is increased while c_m decreases. From **FIGURE 6. (a)** and **FIGURE 6. (b)**, the results reveal that σ_m is increased as c_m is increased. **FIGURE 6. (c)** shows the relation between c_m and σ_m from the simulation results. The horizontal axis of the plot is c_m, and the vertical axis is σ_m. The red dots indicate σ_m for different c_m. The fitting equation is calculated by the least

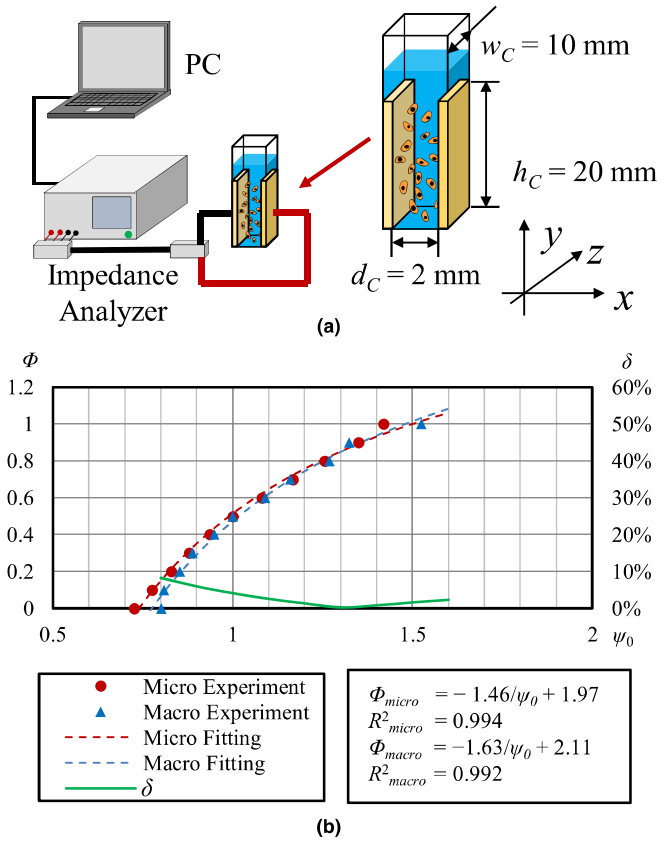

FIGURE 7. Experiment results: (a) experimental setup and macro sensor, (b) $\psi_0 - \Phi$, $\psi_0 - \delta$, and fitting equations.

square method as follows:

$$\sigma_m = 3.17 c_m \tag{16}$$

R^2 of the fitting equation is $R^2 = 0.999$. The result reveals that the relation of c_m and σ_m is linear in a small range of c_m and σ_m.

In addition, $\Phi = 0$ is defined in the case of $c_m = 0.2$ mol/L; $\Phi = 0.5$, $c_m = 0.15$ mol/L; and $\Phi = 0$, $c_m = 0.2$ mol/L. The relation of φ_D and φ_L is expressed as $\varphi_D = 2\varphi_L$ by the calculation of Eq. (15) with the defined c_m in each Φ. **FIGURE 6. (d)** shows the relation between Φ and ψ_1. Based on Eq. (2), the fitting equation is calculated by the least squares method as follows:

$$\Phi = a/\psi_1 + b = -1.5/\psi_1 + 2 \tag{17}$$

where $a = -1.5$ and $b = 2$. R^2 of the fitting equation is $R^2 = 0.999$. In addition, the relation between Φ and ψ_1 is close to that of the experiment result.

B. SENSOR SIZE VERSATILITY

The second discussion point is the sensor size versatility. As shown in **FIGURE 7. (a)**, two rectangular electrodes with a surface area of $A = w_C \times h_C = 10 \times 20$ mm^2 were adopted. The distance between the electrodes is $d_C = 2$ mm. An impedance analyzer (HIOKI IM7850) that supports a scanning frequency range from $f = 100$ kHz to $f = 300$ MHz and a PC (Mouse computer W950JU) were used to measure and record the impedance data. Other experimental conditions were exactly the same as those in the experiment discussed in Chapter III. Based on the experiment results, the relation between ψ_0 and Φ in the case of this macro sensor is also expressed as an empirical equation as follows:

$$\Phi = a/\psi_0 + b = -1.63/\psi_0 + 2.11 \tag{18}$$

where the coefficients $a = -1.63$ and $b = 2.11$, and $R^2 = 0.992$.

In order to quantitate the effect of sensor size, a size effect factor δ is adopted to evaluate the difference between empirical equations of micro and macro sensors, which is defined as follows:

$$\delta(\psi_0) = \left[\frac{\left| \Phi(\psi_0)_{micro} - \Phi(\psi_0)_{macro} \right|}{\mathrm{Max}(\Phi)} \right] \times 100\% \tag{19}$$

where $\Phi(\psi_0)_{micro}$ and $\Phi(\psi_0)_{macro}$ are denoted by the empirical equation in the case of micro and macro electrodes respectively. $\mathrm{Max}(\Phi)$ is the maximum of Φ, $\mathrm{Max}(\Phi) = 1$.

As shown in **FIGURE 7. (b)**, the empirical relation between ψ_0 and Φ in the case of micro and macro sensors shows the same tendency. In the ψ_0 range between $\psi_0 = 0.9$ and $\psi_0 = 1.5$, size effect factor δ is very small at $\delta < 5\%$. This reveals that the sensor size is versatile in the ψ_0 range between $\psi_0 = 0.9$ and $\psi_0 = 1.5$ (in the case that $\Phi(0.9) = 0.2$ and $\Phi(1.5) = 1$).

C. VERSATILITY OF REAL-TIME DETECTION

The third discussion point is the versatility of real-time detection. In order to support real-time detection, the impedances of the medium (Z_{extmed} and $Z_{extmedref}$) are replaced by the impedance of the cell solution (Z_{extm} and $Z_{extmref}$). This is expressed as Eq. (7). The effect of the replacement is clarified by a medium effect factor $\eta(f)$ [%], which is expressed as follows:

$$\eta(f) = \left[1 - \frac{\left| Z''_{med} - Z''_{sol} \right|}{\left| Z''_{sol} \right|} \right] \times 100\% \tag{20}$$

where Z''_{med} is the impedance imaginary part of the medium. Z''_{med} is obtained by measuring the supernatant, which was extracted after centrifuging the cell solution. Z''_{sol} is the impedance imaginary part of the multi-mixed cell solution. A larger value means that Z''_{sol} is similar to Z''_{med}. When η is 100%, σ_{med} is equal to σ_m.

FIGURE 8. (a) shows the condition of the multi-mixed cell solution. Certain concentrations of living and dead cells are mixed at different Φ, and then some of the multi-mixed cell solution is centrifuged to extract the supernatant. After the operation, the cell solution and supernatant at different Φ are detected by EIS in micro and macro sensors.

FIGURE 8. (b) shows the relation between η and f in a micro sensor. From the figure, the range of f at the extremum of the impedance imaginary part for each Φ is from $f = 100$ kHz to $f = 300$ kHz (shown as a dotted ellipse). In this frequency range, $\eta > 95\%$. This result reveals that the effect of the replacement is small and the detection is versatile

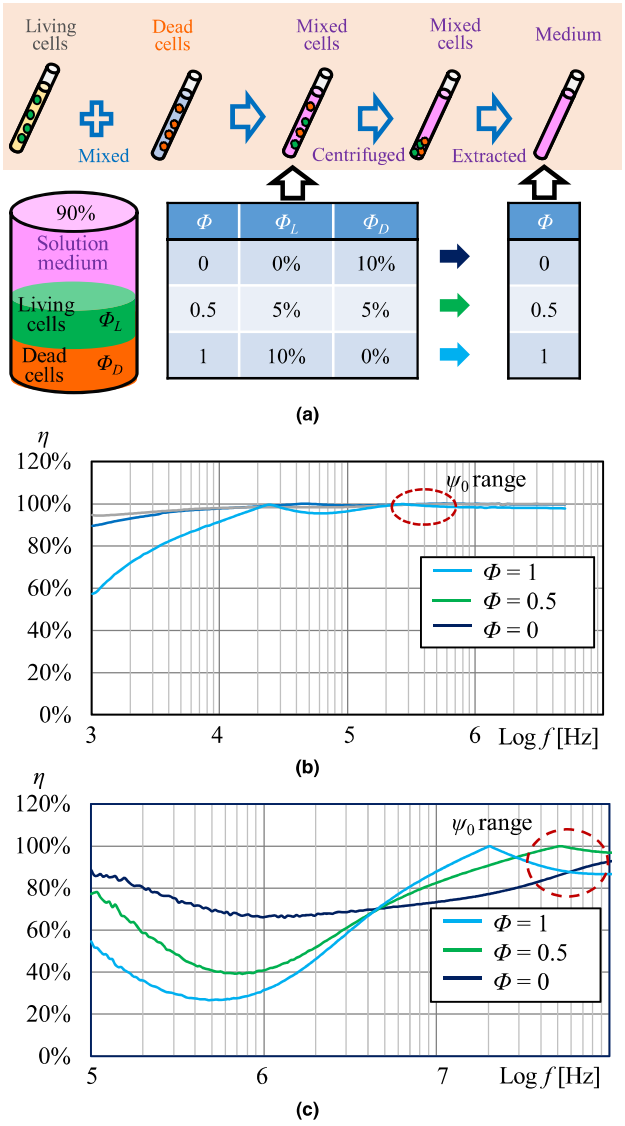

FIGURE 8. Results of replacement: (a) condition of multi-mixed cell solution and their medium, (b) $f - \eta$ in micro sensor, (c) $f - \eta$ in macro sensor.

and highly accurate in the micro sensor. **FIGURE 8. (c)** shows the results of η by f in a macro sensor. From the figure, the range of f at the extremum of the impedance imaginary part for each Φ is from $f = 30$ MHz to $f = 60$ MHz (shown as a dotted ellipse). In this frequency range, $\eta > 85\%$. This result reveals that the effect of the replacement is small and the detection is also versatile. In addition, the accuracy of the macro sensor is lower than the accuracy of the micro sensor.

As shown in **FIGURE 8. (b)** and **FIGURE 8. (c)**, η of the micro sensor is higher than η of the macro sensor. This reveals that it is better to conduct the method with a micro sensor. In addition, the difference between Eq. (8) and Eq. (18) is caused by the different effects of the replacement on the micro and macro sensors.

V. CONCLUSIONS

A novel empirical equation for living cell fraction $\Phi(\psi_0)$ in mixed living and dead cell solution is proposed based on micro EIS.

1) A cell living indicator ψ_0 was defined, and the function of $\Phi(\psi_0)$ was developed by the theoretical relation between the impedance of the solution medium and living cell fraction in the mixed cell solution. The basic form of $\Phi(\psi_0)$ is $\Phi = a/\psi_0 + b$.
2) Experiments were conducted to calculate the empirical coefficient of $\Phi(\psi_0)$ by micro EIS. As a result, $\Phi(\psi_0)$ was indicated as $\Phi = -1.46/\psi_0 + 1.97$ in the case of a total mixed cell concentration $\Phi_{total} = 10$ vol% with a coefficient of determination $R^2 = 0.994$.
3) Simulation results revealed that the theoretical effectiveness of the relation between c_m and σ_m is linear in an ion solution that has a low ion concentration. Meanwhile, the versatility of the sensor size and real-time detection were discussed. The method is suitable and highly accurate in detecting Φ under these conditions.

REFERENCES

[1] J. Guo, X. Huang, and Y. Ai, "On-demand lensless single cell imaging activated by differential resistive pulse sensing," *Anal. Chem.*, vol. 87, no. 13, pp. 6516–6519, 2015.
[2] S. H. Hawkins *et al.*, "Predicting outcomes of nonsmall cell lung cancer using CT image features," *IEEE Access*, vol. 2, pp. 1418–1426, 2014.
[3] E. Fait, A. Gaumann, and M. A. Konerding, "3D microvascular architecture of pre-cancerous lesions and invasive carcinomas of the colon," *Brit. J. Cancer*, vol. 84, no. 10, pp. 1354–1362, 2001.
[4] J. C. Stockert, R. W. Horobin, L. L. Colombo, and A. Blázquez-Castro, "Tetrazolium salts and formazan products in cell biology: Viability assessment, fluorescence imaging, and labeling perspectives," *Acta Histochem.*, vol. 120, no. 3, pp. 159–167, 2018.
[5] N. Arraud, C. Gounou, D. Turpin, and A. R. Brisson, "Fluorescence triggering: A general strategy for enumerating and phenotyping extracellular vesicles by flow cytometry," *Cytometry A*, vol. 89A, no. 2, pp. 184–195, 2016.
[6] G. Kang, S. K. Yoo, H.-I. Kim, and J.-H. Lee, "Differentiation between normal and cancerous cells at the single cell level using 3-D electrode electrical impedance spectroscopy," *IEEE Sensors J.*, vol. 12, no. 5, pp. 1084–1089, May 2012.
[7] M. Al Ahmad, Z. Al Natour, F. Mustafa, and T. A. Rizvi, "Electrical characterization of normal and cancer cells," *IEEE Access*, vol. 6, pp. 25979–25986, 2018.
[8] T. A. York, T. N. Phua, L. Reichelt, A. Pawlowski, and R. Kneer, "A miniature electrical capacitance tomograph," *Meas. Sci. Technol.*, vol. 17, pp. 2119–2129, 2006.
[9] M. Al Ahmad, Z. Al Natour, S. Attoub, and A. H. Hassan, "Monitoring of the budding yeast cell cycle using electrical parameters," *IEEE Access*, vol. 6, pp. 19231–19237, 2018.
[10] B. H. Brown, "Electrical impedance tomography (EIT): A review," *J. Med. Eng. Technol.*, vol. 27, no. 3, pp. 97–108, 2009.
[11] K. H. Han, A. Han, and A. B. Frazier, "Microsystems for isolation and electrophysiological analysis of breast cancer cells from blood," *Biosensors Bioelectron.*, vol. 21, no. 10, pp. 1907–1914, 2006.
[12] J. Yun *et al.*, "Micro electrical impedance spectroscopy on a needle for ex vivo discrimination between human normal and cancer renal tissues," *Biomicrofluidics*, vol. 10, no. 3, 2016, Art. no. 034109.
[13] X. Liu, J. Yao, T. Zhao, H. Obara, Y. Cui, and M. Takei, "Image reconstruction under contact impedance effect in micro electrical impedance tomography sensors," *IEEE Trans. Biomed. Circuits Syst.*, vol. 12, no. 3, pp. 623–631, Jun. 2018.
[14] J. Yao, M. Sugawara, H. Obara, T. Mizutani, and M. Takei, "Distinct motion of GFP-tagged histone expressing cells under AC electrokinetics in electrode-multilayered microfluidic device," *IEEE Trans. Biomed. Circuits Syst.*, vol. 22, no. 6, pp. 1450–1458, Dec. 2017.
[15] Y. Kang, B. Cetin, Z. Wu, and D. Li, "Continuous particle separation with localized AC-dielectrophoresis using embedded electrodes and an insulating hurdle," *Electrochimica Acta*, vol. 54, no. 6, pp. 1715–1720, 2009.

[16] A. P. Andersen, J. M. A. Moreira, and S. F. Pedersen, "Interactions of ion transporters and channels with cancer cell metabolism and the tumour microenvironment," *Philos. Trans. Roy. Soc. B, Biol. Sci.*, vol. 369, no. 1638, 2014, Art. no. 20130098.
[17] R. B. de Souza, R. K. Silva, D. S. Ferreira, S. de Sá Leitão Paiva, Jr., W. de Barros Pita, and M. A. de Morais, Jr., "Magnesium ions in yeast: Setting free the metabolism from glucose catabolite repression," *Metallomics Integr. Biometal Sci.*, vol. 8, no. 11, pp. 1193–1203, 2016.
[18] Y. Ihara-Ohori, M. Nagano, S. Muto, H. Uchimiya, and M. Kawai-Yamada, "Cell death suppressor Arabidopsis bax inhibitor-1 is associated with calmodulin binding and ion homeostasis," *Plant Physiol.*, vol. 143, no. 2, pp. 650–660, 2007.
[19] C. M. A. Brett and A. M. O. Brett, "Electrochemical cells: Thermodynamic properties and electrode potentials," in *Electrochemistry*. Oxford, U.K.: Oxford Univ. Press, 1993, pp. 26–31.
[20] K. Asami, T. Hanai, and N. Koizumi, "Dielectric properties of yeast cells," *J. Membrane Biol.*, vol. 28, no. 1, pp. 169–180, 1976.
[21] O. V. Bobreshova, O. V. Bobylkina, P. I. Kulintsov, G. A. Bobrinskaya, V. P. Varlamov, and S. V. Nemtsev, "Conductivity of aqueous solutions of low-molecular chitosan," *Russian J. Electrochem.*, vol. 40, no. 7, pp. 694–697, 2004.
[22] J. Yao, H. Obara, A. Sapkota, and M. Takei, "Development of three-dimensional integrated microchannel-electrode system to understand the particles' movement with electrokinetics," *Biomicrofluidics*, vol. 10, no. 2, 2016, Art. no. 024105.
[23] T. Zhao, J. Yao, K. Liu, and M. Takei, "Investigation of particle inertial migration in high particle concentration suspension flow by multi-electrodes sensing and Eulerian–Lagrangian simulation in a square microchannel," *Biomicrofluidics*, vol. 10, no. 2, 2016, Art. no. 024120.
[24] J. Yao and M. Takei, "Application of process tomography to multiphase flow measurement in industrial and biomedical fields: A review," *IEEE Sensors J.*, vol. 17, no. 24, pp. 8196–8205, Dec. 2017.
[25] V. F. Lvovich, "Impedance representation of bulk-material and electrode processes," in *Impedance Spectroscopy*. Hoboken, NJ, USA: Wiley, pp. 71–85, 2012.
[26] V. Raicu, C. Gusbeth, D. F. Anghel, and G. Turcu, "Effects of cetyltrimethylammonium bromide (CTAB) surfactant upon the dielectric properties of yeast cells," *Biochim. Biophys. Acta*, vol. 1379, no. 1, pp. 7–15, 1998.
[27] T. Sun, N. G. Green, and H. Morgan, "Analytical and numerical modeling methods for impedance analysis of single cells on-chip," *Nano*, vol. 3, no. 1, pp. 55–63, 2008.
[28] T. Sun and H. Morgan, "Single-cell microfluidic impedance cytometry: A review," *Microfluidics Nanofluidics*, vol. 8, no. 4, pp. 423–443, 2010.

XIAYI LIU received the B.Eng. and M.Sc. degrees from the Xi'an University of Technology, China, in 2011 and 2014, respectively, where he is currently pursuing the Ph.D. degree with the Faculty of Mechanical and Precision Instrument Engineering.

He was an Exchange Student with Chiba University, Japan, from 2016 to 2018. His research interests include bio-microfluidics, multiphase flow dynamics, and electrical impedance tomography.

YAHUI CUI received the B.Eng., M.Sc., and Ph.D. degrees form the Xi'an University of Technology (XUT), Xi'an, China, where he is currently a Professor and the Dean of the Faculty of Mechanical and Precision Instrument Engineering.

He is also an Academic Leader of the Mechanical Design and Theory, XUT, an Executive Director of the National Mechanical Principle Teaching Research, and the Managing Director of the Shaanxi Provincial Institute of Mechanical Engineering. His current research interests include mechanical transmission device and theory, vehicle transmission technology research and vehicle components, and the principle, simulation, and recovery of ancient mechanism.

Dr. Cui is a Senior Member of the Chinese Mechanical Engineering Society.

TONG ZHAO received the B.S. and M.S. degrees in mechanical engineering from the Xi'an University of Technology (XUT), Xi'an, China, in 2003 and 2006, respectively, and the Ph.D. degree in mechanical engineering from Nihon University, Tokyo, Japan, in 2010, where he was a Research Assistant, from 2010 and 2011.

From 2013 to 2015, he was a Fellow of the Japanese Society for Promotion of Science, Chiba University, Chiba, Japan. He is currently an Associate Professor with the School of Mechanical and Precision Instrument Engineering, XUT. His current research interests include the measurement and numerical simulation of multiphase flow and corresponding multicomponent heat transfer mechanism.

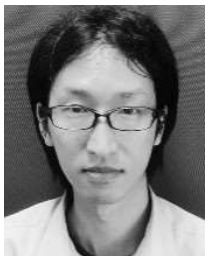

DAISUKE KAWASHIMA received the B.S., M.S., and Ph.D. degrees in mechanical engineering from the Tokyo Metropolitan Institute of Technology, Tokyo, Japan, in 2012, 2014, and 2017, respectively.

Since 2017, he has been a Postdoctoral Fellow with Chiba University, Chiba, Japan. His research interests include heat and mass transfer in microchannel, optical measurement using near-infrared spectroscopy, and electrical measurement applying to the medical and industrial fields.

HIROMICHI OBARA received the B.Eng., M.Sc., and Ph.D. degrees from the Tokyo Metropolitan Institute of Technology, Tokyo, Japan, where he was an Assistant Professor, from 1998 to 2005.

From 2001 to 2002, he was a Guest Researcher at NIST, USA. He is currently an Associate Professor with the Department of Mechanical Engineering, Tokyo Metropolitan University, Japan. His research interests include fluid engineering, bioengineering, electrokinetics, and organ engineering.

MASAHIRO TAKEI received the B.Eng., M.Sc., and Ph.D. degrees from Waseda University, Tokyo, Japan.

He was with University Leeds as a Guest Researcher in the U.K., by the Royal Society, U.K., in 2007. He is currently a Professor and the Vice Dean of the Graduate School of Engineering, Chiba University, Japan. His research interests include multiphase flow dynamics, visualization and measurement, process tomography and inverse problem, microfluidics and bio application.

Dr. Takei is the President of the International Society for Industrial Process Tomography (Headquarter: U.K.), a Vice Chair Person, a Board Member of the American Society of Mechanical Engineers Japan Section, a Board Member of the Visualization Society of Japan, a Councilor of the Society of Powder Technology, Japan, a Board Member of the Japanese Society Experimental Mechanics, a Guest Editor of *Measurement Science and Technology* published by the Institute of Physics, a Guest Editor of *Flow Measurement and Instrumentation* (Elsevier), and an Editorial Board Member of the *Journal of Visualization* (Springer).